Dalton Transactions

ROYAL SOCIETY OF CHEMISTRY

PAPER

View Article Online
View Journal | View Issue

Check for updates

Cite this: *Dalton Trans.*, 2023, **52**, 16886

Chlorinated polyhedral selenaboranes revisited by joint experimental/computational efforts: the formation of *closo*-1-SeB_9Cl_9 and the crystal structure of *closo*-$SeB_{11}Cl_{11}$†

Willi Keller,*[a] Matthias Hofmann,[b] Hubert Wadepohl,[b] Markus Enders,[b] Jindřich Fanfrlík[c] and Drahomír Hnyk*[d]

The recent success in the formation of chlorinated telluraboranes and the reactivities of pnictogenaboranes prompted us to re-examine the vacuum co-pyrolysis of B_2Cl_4 with Se_2Cl_2 at various molar ratios and temperatures in order to search for the generation of other polyhedral selenaboranes than *closo*-SeB_5Cl_5 (**1a**) and *closo*-$SeB_{11}Cl_{11}$ (**1b**), the latter being observed earlier. Interestingly, a new compound with the elemental composition SeB_9Cl_9 (**2**) was detected, this time by high- and low-resolution mass spectrometry. Further characterization by 1- and 2-D ^{11}B-NMR spectroscopy suggests that **2** should adopt a closed bicapped square-antiprismatic geometry with selenium at the apical position. Moreover, vacuum sublimation gave suitable crystals of **1b**, which were subjected to single-crystal X-ray structure determination. Crystallographic data analysis confirmed that **1b**, consistent with its 26 skeletal electron count, adopts a distorted icosahedral structure close to the symmetry of C_{5v}. Computations at the DFT-D3 level have revealed that 33% of the total computed binding motifs in the grown **1b** crystals are due to the very strong chalcogen bonding. Moreover, SAPT decomposition has shown that the bonding motifs in the crystals are stabilized mainly by dispersion and electrostatic terms. Homodecoupling and high resolution ^{11}B NMR and ^{77}Se NMR experiments have resolved both coupling constants $^1J(^{11}B^{11}B)$ and $^1J(^{77}Se^{11}B)$ as well as the ^{77}Se chemical shift of **1a** and **1b**, which are in reasonable agreement with the corresponding computed values. The computed ^{11}B chemical shifts of **2** were determined by the well-established DFT/GIAO/NMR structural tool based on its B3LYP/6-311+G** internal coordinates. They agree well with the experimental values and provide a good representation of the molecular structure of **2** in solution. The extraordinary downfield ^{11}B NMR chemical shift of B(10) in **2** has been ascribed to the intensive paramagnetic contribution to the shielding tensor in this bicapped square-antiprismatic motif. Calculations of the synproportionation free energies of smaller (n − 1) *closo*-selenaboranes with larger-sized (n + 1) ones support the extraordinary stability of octahedral, bicapped square-antiprismatic and icosahedral *closo* motifs in the SeB_nCl_n family (n = 4–12).

Received 13th September 2023,
Accepted 18th October 2023

DOI: 10.1039/d3dt02987e

rsc.li/dalton

Introduction

Polyhedral borane and heteroborane clusters are known for the presence of delocalized electron-deficient bonding[1] and characterized by forming three-center, two-electron (3c–2e) bonds. This bonding is quite different from the organic chemistry that is dominated by classical two-center, two-electron (2c–2e) bonds. The trigonal faces of boranes and the so-called heteroboranes are assembled to create various three-dimensional shapes. There exist *closo*-, *nido*-, *arachno*- and *hypho*-type cages according to the so-called electron count.[2] The *closo*-systems belong to the most researched clusters predominantly represented, *e.g.* by octahedral *closo*-$B_6H_6^{2-}$, bicapped square-antiprismatic *closo*-$B_{10}H_{10}^{2-}$ and icosahedral *closo*-$B_{12}H_{12}^{2-}$,

[a]*Institut für Chemie, Universität Hohenheim, Garbenstrasse 30, 70599 Stuttgart, Germany. E-mail: willi.keller@uni-hohenheim.de*
[b]*Anorganisch-Chemisches Institut, Ruprecht-Karls-Universität Heidelberg, Im Neuenheimer Feld 270, 69120 Heidelberg, Germany*
[c]*Institute of Organic Chemistry and Biochemistry of the Czech Academy of Sciences, Flemingovo nám. 2, 166 10 Praha 6, Czech Republic*
[d]*Institute of Inorganic Chemistry of the Czech Academy of Sciences, 250 68 Husinec-Řež, Czech Republic. E-mail: hnyk@iic.cas.cz*

†Electronic supplementary information (ESI) available: Descriptions of experiments, computational and crystallographic details, ^{11}B and ^{77}Se NMR spectra, and ESI-MS spectra. CCDC 2251721. For ESI and crystallographic data in CIF or other electronic format see DOI: https://doi.org/10.1039/d3dt02987e

recognized as well-designed building blocks of boron cluster chemistry.[3] The systematic replacement of formally neutral BX vertices in the *closo*-$B_nX_n^{2-}$ (X = H and/or halogens, n = 6, 10, 12) can lead to a variety of n-vertex *closo*-heteroboranes, either the parent or with terminal halogens. For example, isoelectrolobal vertices such as E (E = S, Se, Te) with a formal charge of +2 give rise to *closo*-1-EB_nX_n (n = 5, 9, 11), known as chalcogenaboranes.[3] Conceivably, there is a sort of similarity of such 3D chalcogenaboranes with 2D heterocyclic compounds exemplified by thiophene, selenophene, *etc*. The presence of chalcogens in suitably designed structural moieties results in the detection of the so-called chalcogen bonds responsible for crystal packing not only for chalcogenaboranes.[4–6] However, the area of chalcogenaboranes turned out to be underresearched and just a few polyhedral selenaboranes $Se_xB_yH_z$ are known.[7] Recently, we have reported on the synthesis and DFT/GIAO/NMR study of the perhalogenated selenaboranes *closo*-SeB_5Cl_5 (**1a**) and *closo*-$SeB_{11}Cl_{11}$ (**1b**) by the co-pyrolysis reaction of a 9 : 1 mixture of B_2Cl_4 with Se_2Cl_2 *in vacuo* at 330 °C.[8] It is well known from the thermal disproportionation reactions of B_2Cl_4 with n-vertex boron subchlorides B_nCl_n (n = 8–12)[9] that the size n and the distribution of products strongly depend on the reaction temperature and time under thermolytic conditions: higher pyrolysis temperatures augment the amount of active BCl species (see eqn (1)) and thus increase the probability of the formation of larger cages. In the co-pyrolysis of B_2X_4 (X = Cl, Br) with phosphorus trihalide PX_3 (X = Cl, Br), it has been shown that the formation of the main product, *closo*-1,2-$P_2B_4X_4$ (X = Cl,[10a] X = Br [10b,c]), is accompanied by the larger homologs *closo*-1,10-$P_2B_8Cl_8$ [10d] and *closo*-1,7-$P_2B_{10}X_{10}$ (X = Cl,[10d] X = Br [10e]) as well as *conjuncto*-3,3′-$(1,2\text{-}P_2B_4X_3)_2$ (X = Cl,[10d] X = Br [10e]) when the temperature rises from 330 °C to 400 °C and when the molar B_2Cl_4 content is augmented. Furthermore, extensions of the geometric motifs formed by co-pyrolysis reactions have been found with exoskeletal dihaloboryl groups in perhalogenated carboranes.[11] In order to create new homologs of polyhedral selenaboranes, we have now reexamined the co-pyrolysis reaction of B_2Cl_4 with Se_2Cl_2 both by increasing the temperature and by altering the molar ratio of the reactants with respect to the conditions of our previous report. Under such conditions, a novel chlorinated selenaborane, *i.e.* *closo*-1-SeB_9Cl_9 (**2**) (Fig. 1), has now been detected. In addition, it was our intention to extend the still quite limited spectroscopic data of *closo*-SeB_5Cl_5 and *closo*-$SeB_{11}Cl_{11}$ available so far to allow comparisons with the data of the very recently reported related octahedral and icosahedral *closo*-telluraboranes.[12]

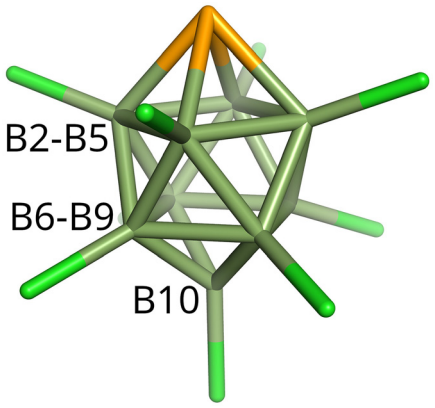

Fig. 1 A molecular diagram of *closo*-1-SeB_9Cl_9 (**2**) of a symmetry of C_{4v}. Salient interatomic distances are (in Å at B3LYP/6-311+G**): r[Se–B(2)] 2.127, r[B(2)–B(3)] 2.013, r[B(2)–B(6)] 1.895, and r[B(6)–B(10)] 1.714.

Results and discussion

It has been shown in all previous formations of heteroboranes *via* co-pyrolysis of B_2X_4 with elemental halides *in vacuo* that the incorporation of heteroatoms can only occur in the gas phase,[10,12] and therefore the temperature during pyrolysis has to be high enough to vaporize both starting components, but not too high to cause the thermal degradation of the prospected heteroborane products (*e.g.* as a reverse reaction of eqn (4)). Under pyrolytic conditions, both Se_2Cl_2 and B_2Cl_4 are unstable and disproportionate to elemental selenium (eqn (3))[13] and intermediate [BCl] species[14] (eqn (1)), from which the latter can aggregate to boron subchlorides B_nCl_n (n = 8–12, eqn (2))[9] in a homo-component reaction or incorporate selenium into condensing [BCl] particles to the selenaborane products (eqn (4) and (5)) in hetero-component reactions.

We have now reexamined the co-pyrolysis of B_2Cl_4 with Se_2Cl_2 *in vacuo* (10^{-3} mbar) by altering both the temperature and molar conditions of our first report from 330 °C and 9 : 1 to (a) 350 °C and 7 : 1 or (b) 400 °C and 10 : 1. After the reaction, the product mixtures were thoroughly extracted with liquid BCl_3, after which the extractant was evaporated *in vacuo*. The residues were separated into the two fractions volatile upon heating to $T \approx 180$ °C *in vacuo* or volatile between $T \approx 180$ °C and $T \approx 350$ °C under these conditions, and were analyzed by ^{11}B NMR spectroscopy and mass spectrometry.

Both experiments revealed the formation of *closo*-selenaboranes and boron subhalides B_nCl_n (n = 8–11), the latter consisting mainly of B_9Cl_9. The selenaborane portion in case (a) contained approximately equal amounts of *closo*-SeB_5Cl_5 (**1a**) in the more volatile fraction and *closo*-$SeB_{11}Cl_{11}$ (**1b**) together with smaller amounts of *closo*-1-SeB_9Cl_9 (**2**) in the less volatile fraction. In case (b), the more volatile fraction contained only very small amounts of **1a**, while the less volatile fraction contained **1b** in amounts that were approximately the same as in case (a). **2** could not be detected in (b). These results indicate that the generation of selenaborane **1a** is favored both by a lower pyrolysis temperature and by a lower molar content of B_2Cl_4 in the starting mixture compared with the formation of **1b**. **2** requires temperatures as high as 350 °C for formation. Due to their similar volatilities compared to those of the boron subhalide side-products B_nCl_n, the selenaboranes **1a**, **1b** and **2** could not be completely separated by vacuum fractionation, where they sublimed as white solids at approximately 50 °C

(**1a**), 200 °C (**2**) and 350 °C (**1b**), respectively. The final crystallization step for the isolation of **1a** and **1b** afforded a slow cooling of the sealed, evacuated samples from 200 °C (for **1a**) or 350 °C (for **1b**) to room temperature over a period of 20 h. However, from the obtained crystalline materials, only crystals of **1b** were suitable for X-ray diffraction analysis. Selenaborane **2** could only be enriched by the extraction of the less volatile fraction with BCl_3. Selenaboranes **1a**, **1b** and **2** are soluble in common aprotic hydrocarbon solvents, such as benzene, toluene, methylene chloride and chloroform. They are thermally stable at least up to their formation temperature, *i.e.* 400 °C.

Eqn (4) and (5) describe the overall conversion, but not the course of molecular formation and possible side reactions. Based on eqn (5), the gross yield of **2** was only 1%.

$$n\mathrm{B_2Cl_4} \rightarrow n[\mathrm{BCl}] + n\mathrm{BCl_3} \quad (1)$$

$$n[\mathrm{BCl}] \rightarrow \mathrm{B}_n\mathrm{Cl}_n \quad (n = 8\text{–}12) \quad (2)$$

$$2\mathrm{Se_2Cl_2} \leftrightharpoons 3\mathrm{Se} + \mathrm{SeCl_4} \quad (3)$$

$$\mathrm{Se} + n[\mathrm{BCl}] \rightarrow \mathrm{SeB}_n\mathrm{Cl}_n \quad (4)$$

$$19\mathrm{B_2Cl_4} + \mathrm{Se_2Cl_2} \rightarrow 2\mathrm{SeB_9Cl_9}(\mathbf{2}) + 20\mathrm{BCl_3} \quad (5)$$

In order to predict the relative stability of each member of the *closo*-SeB_nCl_n family (n = 4–12), we calculated the "synproportionation" energies of reactions between a smaller (n − 1) and a larger (n + 1) selenaborane according to eqn. (6)–(12) to form the member with the number n of B–Cl vertices in between at the B3LYP/6-311+G**+ZPE level. The computations of these energy balances use the most stable positional isomers within a particular *closo*-selenaborane (for the individual molecular shapes, see also ref. 15). These computations strongly support the extraordinary stabilities of octahedral, bicapped square-antiprismatic and icosahedral *closo* motifs, which is fully consistent with the trend observed for perhydrogenated carboranes[16] and perchlorinated phosphaboranes.[10d]

$$1\text{-}\mathrm{SeB_4Cl_4} + 2\text{-}\mathrm{SeB_6Cl_6} \rightarrow 2\ \mathrm{SeB_5Cl_5}(\mathbf{1a}) \quad \mathbf{-19.7} \quad (6)$$

$$\mathrm{SeB_5Cl_5}(\mathbf{1a}) + 1\text{-}\mathrm{SeB_7Cl_7} \rightarrow 2\ 2\text{-}\mathrm{SeB_6Cl_6} \quad 0.3 \quad (7)$$

$$2\text{-}\mathrm{SeB_6Cl_6} + 1\text{-}\mathrm{SeB_8Cl_8} \rightarrow 2\ 1\text{-}\mathrm{SeB_7Cl_7} \quad 1.8 \quad (8)$$

$$1\text{-}\mathrm{SeB_7Cl_7} + 1\text{-}\mathrm{SeB_9Cl_9}(\mathbf{2}) \rightarrow 2\ 1\text{-}\mathrm{SeB_8Cl_8} \quad 13.7 \quad (9)$$

$$1\text{-}\mathrm{SeB_8Cl_8} + 2\text{-}\mathrm{SeB_{10}Cl_{10}} \rightarrow 2\ 1\text{-}\mathrm{SeB_9Cl_9}(\mathbf{2}) \quad \mathbf{-18.8} \quad (10)$$

$$1\text{-}\mathrm{SeB_9Cl_9}(\mathbf{2}) + \mathrm{SeB_{11}Cl_{11}}(\mathbf{1b}) \rightarrow 2\ 2\text{-}\mathrm{SeB_{10}Cl_{10}} \quad 38.2 \quad (11)$$

$$2\text{-}\mathrm{SeB_{10}Cl_{10}} + 2\text{-}\mathrm{SeB_{12}Cl_{12}} \rightarrow 2\ \mathrm{SeB_{11}Cl_{11}}(\mathbf{1b}) \quad \mathbf{-68.8}(12) \quad (12)$$

The ^{11}B experimental and computed chemical shifts of **1a** and **1b** have already been given in our previous report, but as experimental ones without specifications. In analogy with *closo*-TeB_5Cl_5,[12] the ^{11}B NMR spectrum of **1a** shows the reported two broad signals in a 1 : 4 ratio at 23.2 ppm ($h_{1/2} \approx$ 110 Hz) for B(6) and at 4.6 ppm for B(2–5) with the expected cross-peak in the COSY ^{11}B^{11}B NMR spectrum. The latter signal resolves to a quartet either by homodecoupling or by applying the Lorentz–Gaussian transformation with a $^1J(^{11}\mathrm{B}^{11}\mathrm{B})$ of 27 Hz (the computed J value is 30.6 Hz, see below and the ESI†), thereby indicating coupling with B(6). Satellites of the signal at 4.6 ppm assume the coupling of B(2–5) with selenium, given by $^1J(^{77}\mathrm{Se}^{11}\mathrm{B}) \approx 36.5$ Hz (the computed K value is 22 Hz, see below and the ESI†). The ^{77}Se NMR signal of **1a** is very broad ($h_{1/2} \approx 236$ Hz) due to the scalar interaction of ^{77}Se with the ^{11}B (and ^{10}B) of B(2–5) at −149 ppm (see below for the computed value).

The ^{11}B NMR spectrum of **1b** shows the reported three signals in a 5 : 5 : 1 ratio at −3.3 (B7–11), 3.9 ppm (B2–6) and 17.3 ppm (B12) and the cross-peaks between B(7–11)/B(2–6) and B(7–11)/B(12) in the ^{11}B^{11}B COSY NMR spectrum. The individual values indicate the same trend as in the parent *closo*-$SeB_{11}H_{11}$.[7e] The ^{77}Se NMR signal of **1b** is very broad ($h_{1/2} \approx 220$ Hz) due to the scalar interaction of ^{77}Se with the ^{11}B (and ^{10}B) of B(2–6) at −31 ppm (see below for the computed value).

The ^{11}B NMR spectrum of **2** consists of three signals in an approximately 4 : 4 : 1 ratio at 1.7 ppm, 16.8 ppm and 53.0 ppm (for the computed values, see Table 3). The signal at 1.7 ppm shows ^{11}B^{11}B cross-peak correlation with the other two signals and thus can be assigned to B(6–9), the signal at 16.8 ppm can be assigned to B(2–5), and the intensity-one signal at 53.0 ppm (also indicative of its very strong antipodal downfield shift) can be assigned to B(10). The chemical shifts and assignments of **2** are in agreement with those established for the corresponding parent selenaborane *closo*-1-SeB_9H_9,[7f] namely −19.9 ppm (B(6–9)), −5.4 ppm (B(2–5)) and +73.3 ppm (B(10)), with the last one representing an extreme value of antipodal deshielding. This effect has already been explained in relation to the $\delta(^{11}\mathrm{B})$ of B(10) in *closo*-1-SB_9H_9 to the much less pronounced downfield chemical shift of B(12) in *closo*-$SB_{11}H_{11}$.[17]

The mass spectrum of selenaborane **2** exhibits a strong parent ion envelope with minor cut-offs, indicating the stepwise abstraction of BCl_2 and BCl_3 fragments, whose intensity patterns are consistent with the calculated spectra based on natural isotopic abundances.

On the basis of the NMR data and simple skeletal-electron counting rules,[2] **2** should adopt a bicapped square-antiprismatic geometry with selenium on apical position 1 contributing four electrons and each B–Cl unit two electrons to the cluster bonding.

Vacuum sublimation has given suitable crystals of **1b**, which could be subjected to one of the rare examples of the single-crystal X-ray structure determination of a reported selenaborane.

The compound crystallizes in the non-centrosymmetric space group $P2_1$ with two crystallographically independent molecules of essentially identical geometry in the asymmetric unit (Fig. 2). In contrast to the structure of *closo*-TeB_5Cl_5,[12] there are no signs of modulation.

As expected, the crystal packing forces in the crystals of **1b** cause a slight deviation from the symmetry of C_{5v} adopted for a single molecule of this perchlorinated icosahedral selenaborane. Some important bond lengths are collected in Tables 1 and 2. There are two notable geometrical trends: first, a

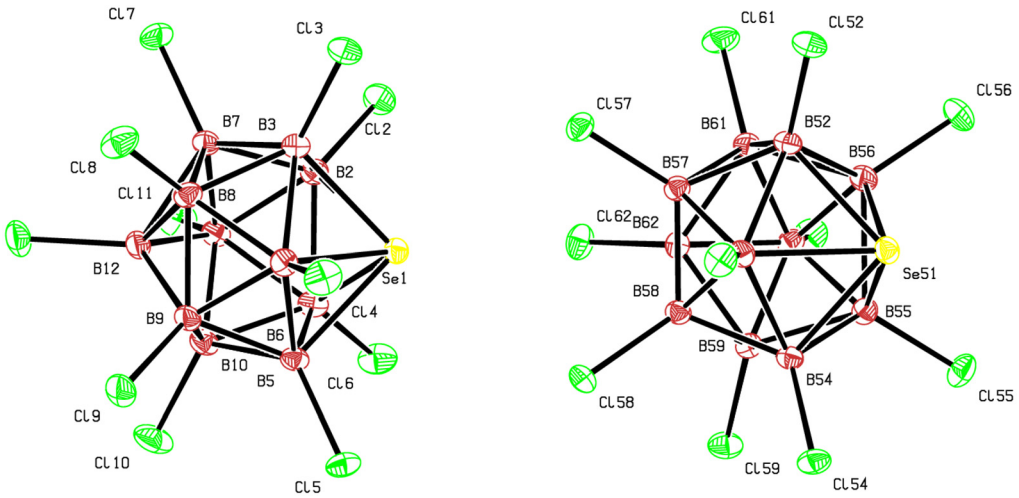

Fig. 2 ORTEP plots of the molecular structure of **1b**. For a compilation of salient bond lengths (*r*, Å), see Tables 1 and 2.

Table 1 B–B bond lengths [Å] in **1b**. The values in square brackets refer to the second independent molecule

Atoms involved	Range	Mean
{B(2)···B(6)}–{B(2)···B(6)}	1.928(3) [1.935(3)]···1.945(3) [1.946(3)]	1.938(6) [1.942(4)]
{B(7)···B(11)}–{B(7)···B(11)}	1.805(4) [1.810(3)]···1.819(3) [1.814(3)]	1.812(5) [1.812(1)]
{B(7)···B(11)}–B(12)	1.789(4) [1.791(3)]···1.797(4) [1.802(3)]	1.793(3) [1.796(4)]
{B(2)···B(6)}–{B(7)···B(11)}	1.769(4) [1.772(4)]···1.779(3) [1.782(3)]	1.774(3) [1.776(3)]

Table 2 B–Cl bond lengths [Å] in **1b**. The values in square brackets refer to the second independent molecule

Bond(s)	Range	Mean
B(2)–Cl(2)···B(6)–Cl(6)	1.740(3) [1.736(2)]···1.746(2) [1.744(2)]	1.744(2) [1.741(3)]
B(7)–Cl(7)···B(11)–Cl(11)	1.757(2) [1.761(2)]···1.775(2) [1.772(2)]	1.765(6) [1.766(5)]
B(12)–Cl(12)	1.768(3) [1.762(2)]	

decrease in the B–B bond lengths with increasing distance from the Se atom, and second, a shortening of the B–Cl distances involving boron atoms bound to Se with respect to the others. Se–B bonds range from 2.166(2) to 2.175(2) Å [mean 2.169(3) Å] in molecule 1 and from 2.162(2) to 2.172(2) Å [mean 2.168(3) Å] in molecule 2. These values are significantly longer than those reported for the gas-phase structure of the parent compound *closo*-$SeB_{11}H_{11}$ (2.129(2) Å),[7e] see also Fig. 2.

The shape of the solid-state structure of **1b** agrees with that already computed at the B3LYP/6-311+G** level of theory[8] and with the gas-phase structures of the corresponding icosahedral chalcogenaborane hydrides *closo*-$EB_{11}H_{11}$ (E = Se, S) based on gas-phase electron diffraction (E = Se,[7e] S [18a]) and microwave spectroscopy (E = S [18b]). However, due to the entirely different physical meanings of the interatomic distances derived using the structural tools mentioned above, the direct comparison must be taken with caution.

We have also examined the bonding motifs and electrostatic properties of **1a**, **1b** and **2** in bonding in terms of employing intrinsic bond orbitals (IBOs) and electrostatic potential (ESP) molecular surfaces in line with the earlier use of this class of materials.[19,20] As shown in Fig. 3, the ESP computations of **1a**, **1b** and **2** provide different patterns. The IBO charges on Se are 0.43 for **1a**, 0.57 for **1b** and 0.69 for **2**. The application of the IBO approach has revealed the nature of bonding in these chlorinated selenaboranes (see Fig. 4 for example). The selenium atom seems to play a decisive role in the three kinds of IBOs in each of these three systems. According to the expansion coefficients (ECs: contributions from individual atoms to a particular IBO to illustrate the nature of such orbitals) associated with the contributions of individual atoms to these orbitals, they may be grouped as follows: there are two emerging IBOs with ECs (the contributing atoms in parentheses) such as 1.05 (Se), 0.52 (B) and 0.25 (B) as well as one IBO with ECs of 1.19 (Se), 0.57 (B) and 0.10 (B) in **1a**. Whereas the first pair of IBOs may be considered of almost a 3c–2e nature, the second one is more or less of the 2c–2e-type. In **1b**, the three IBOs in which Se is involved have the following ECs (the contributing atoms in parentheses): 1.07 (Se), 0.52 (B), 0.20 (B), and 0.12 (B); 1.07 (Se), 0.42 (B), and

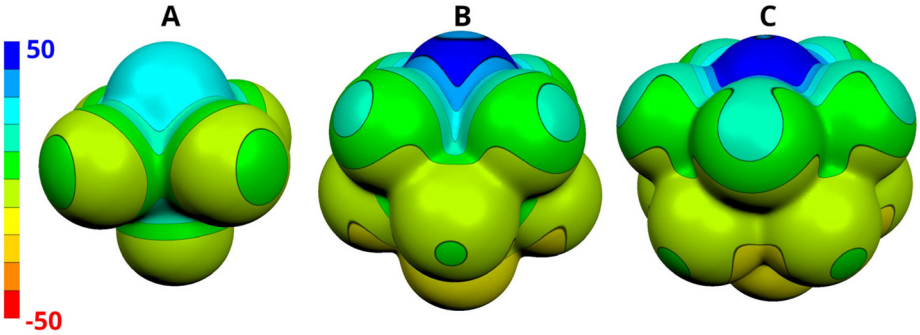

Fig. 3 Computed electrostatic potentials (ESPs) on the 0.001 a.u. molecular surfaces of *closo*-SeB_5Cl_5 (**1a**, A), *closo*-1-SeB_9Cl_9 (**2**, B) and *closo*-$SeB_{11}Cl_{11}$ (**1b**, C). The ESP color range is in kcal mol^{-1}.

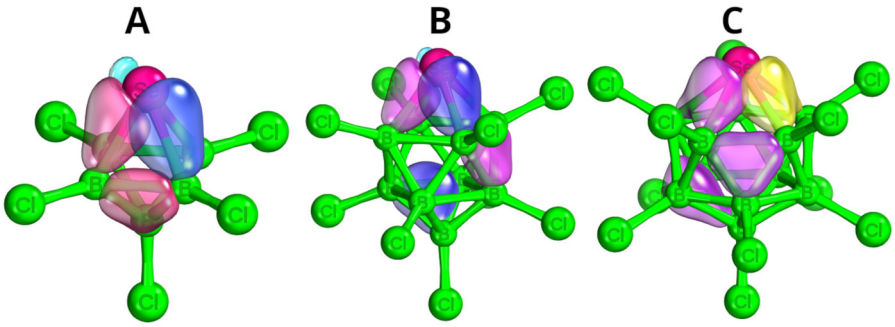

Fig. 4 Examples of bonding in *closo*-SeB_5Cl_5 (**1a**, A), *closo*-1-SeB_9Cl_9 (**2**, B) and *closo*-$SeB_{11}Cl_{11}$ (**1b**, C) as revealed by the application of the IBO computational approach. Color coding: blue – 2c–2e, pink – 3c–2e, and yellow – 4c–2e.

0.37 (B); 1.07 (Se), 0.49 (B) and 0.27 (B). While the first IBO may be viewed as an orbital somewhere between 4c–2e and 2c–2e, the other two are of a 3c–2e nature. Finally, the bonding in the newly formed **2** is also based on the three IBOs grouped in two patterns, *i.e.* one of a 2c–2e nature with the ECs 1.15 (Se) and 0.56 (B) and two of the 3c–2e-type with the ECs 1.1 (Se), 0.54 (B) and 0.26 (B). The bonding in the other hemispheres (and between the hemispheres in **1b** and **2**) is predominantly of a 3c–2e nature, and the corresponding ECs are in the range of *ca.* 0.50–0.70. All the relevant computational details are provided in the ESI.†

It is the σ-hole concept that connects the popular halogen bonding with chalcogen, pnictogen bondings and other related noncovalent interactions.[21] The σ-hole is characterized by its magnitude, abbreviated as $V_{s,max}$. $V_{s,max}$ is defined as the value of the most positive ESP of an electron density surface. Thus, the $V_{s,max}$ values of *closo*-SeB_5Cl_5 (**1a**), *closo*-1-SeB_9Cl_9 (**2**) and *closo*-$SeB_{11}Cl_{11}$ (**1b**) are computed to be 25.8, 41.1 and 44.8 kcal mol^{-1}, respectively. The last result shows that the icosahedral perchlorinated selenaborane has a more positive $V_{s,max}$ than *closo*-$SeB_{11}H_{11}$ ($V_{s,max}$ of 29.5 kcal mol^{-1}).[22] The last value is comparable with that of *nido*-7,8,9,11-$Sb_2C_2B_7H_9$ ($V_{s,max}$ of 42.7 kcal mol^{-1})[23] and explains why the chalcogen bonding[24] in **1b** is so strong in terms of the crystal packing of the corresponding solid-state structure.

The above B3LYP/6-311+G** geometry of **2** has also been used in NMR shift computations using the GIAO-PBE1PBE model chemistry with the same basis set as in the derivation of the molecular geometry of **2**, likewise successfully utilized in previous studies.[12,20] The most striking feature of the molecular geometry of **2** is the considerable expansion of the square belt adjacent to selenium (see Fig. 1), with the analogical pentagonal belt adjacent to Se in **1b** exhibiting the same pattern.

We have also provided the computed ^{77}Se NMR chemical shifts (in ppm, with respect to Me_2Se; experimental values of compounds **1a** and **1b** are given in parentheses; see Table 3),[25] which are nicely related to the experimental values. The ^{11}B NMR chemical shifts of **2** at the same GIAO-PBE1PBE//B3LYP/6-311+G** level are computed as shown in Table 3. Note that B(10) in **2** resonates at *ca.* 20 ppm less (in the upfield direction) with respect to the parent *closo*-1-SB_9H_9.[17] Basically, there is very good agreement with the computed values, *i.e.* the B3LYP/6-311+G** internal coordinates represent a very good approximation of the molecular geometry of **2** in solution.

The most striking feature of the electronic structure of **2** is the resonation of the B(10) vertex in the ^{11}B NMR spectrum at a frequency of *ca.* 52 ppm. This is a result of the intensive paramagnetic contribution to the shielding tensor in this bicapped square-antiprismatic system. Such a contribution arises from

Table 3 Computed[a] and experimental ^{77}Se and ^{11}B chemical shifts with respect to $BF_3.OEt_2$ and Me_2Se, respectively, for a series of bicapped square-antiprismatic, octahedral, and icosahedral selenaboranes

Bicapped square-antiprismatic motifs				
	Se	B(2–5)	B(6–9)	B(10)
2	−511	16.6	−1.9	51.2
Exp.	—	*16.8*	*1.7*	*52.3*
closo-SeB_9H_9	−231	−5.9	−23.5	78.0
Exp.[b]	—	*−5.4*	*−19.9*	*73.3*
10-Cl-*closo*-SeB_9H_8	−519	−9.4	−24.7	76.0
Octahedral motifs				
	Se	B(2–5)		B(6)
1a	−216	5.5[c]		18.2[c]
Exp.	*−146.2*	*4.6*[d]		*23.2*[d]
closo-SeB_5H_5	45	4.8		31.9
6-Cl-*closo*-SeB_5H_4	−406	1.7		26.6
Icosahedral motifs				
	Se	B(2–6)	B(7–11)	B(12)
1b	−92	3.4[c]	−7.0[c]	14.4[c]
Exp.	*−31*	*3.9*[d]	*−3.3*[d]	*17.3*[d]
closo-$SeB_{11}H_{11}$	213	−3.8[e]	−5.9[e]	25.2[e]
12-Cl-*closo*-$SeB_{11}H_{10}$	−57	−5.4	7.0	29.1

[a] GIAO-PBE1PBE//B3LYP/6-311+G**. [b] From ref. 7*f*. [c] The computed ^{11}B chemical shifts are compatible with those derived at GIAO-B3LYP//B3LYP/6-311+G** given in ref. 1. [d] The experimental chemical shifts are compatible with those given in ref. 8, see also the ESI.† [e] The computed ^{11}B chemical shifts are compatible with those given in ref. 7*e* and with the experimental values reported therein.

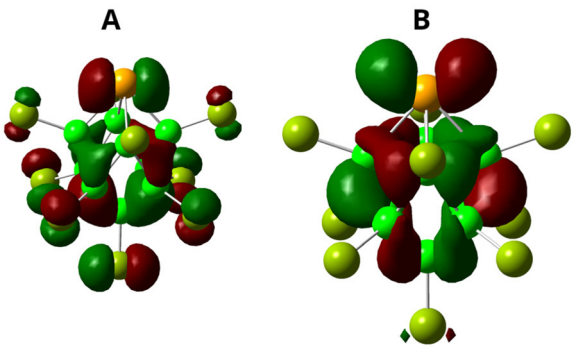

Fig. 5 The HOMO (A) and the LUMO (B) of *closo*-1-SeB_9Cl_9 (**2**).

the coupling of suitably occupied and unoccupied MOs, *i.e.* the HOMO and the LUMO, with large coefficients on the antipodal atom B(10). For this overlap in **2**, see Fig. 5. This explanation is also valid in the case of *closo*-1-SB_9H_9, where the overlap is even more pronounced, which is in line with the higher downfield ^{11}B NMR chemical shift of this atom, namely *ca.* 75 ppm. Interestingly, there is a significant correlation between δ's (^{77}Se) and δ's (^{11}B-antipodal) for **1a**, **1b**, and **2** (see Scheme 1), which indicates a direct transformation of the electron density from an obviously deshielded antipodal boron

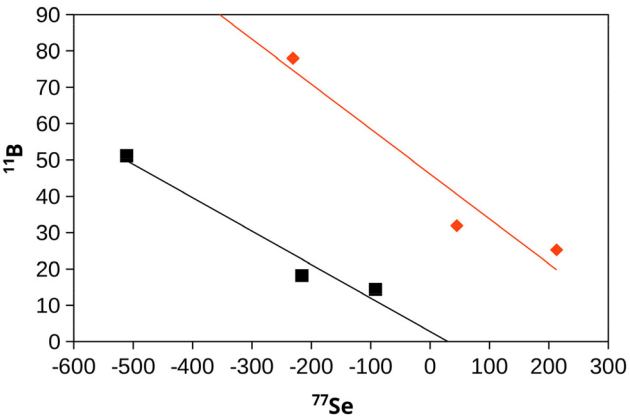

Scheme 1 Correlation between δ's (^{77}Se) and δ's (^{11}B-antipodal) for **1a**, **1b**, and **2** (in black, r^2 = 0.96) and that for their hydrogen-based analogues (in red, r^2 = 0.93).

atom towards the shielded selenium through the corresponding body diagonal. The latter observation might serve as an additional proof of the antipodal effect for these three structural motifs. On the selenium bicapped square-antiprismatic front, we have also looked at *closo*-1-SeB_9H_9, for which the ^{11}B chemical shifts are known.[7f] The downfield shift of B(10) in the latter compound is even larger than that in **2** and also that in *closo*-1-SB_9H_9 mentioned earlier, see also Table 3. In contrast, the computed upfield shift of ^{77}Se is less pronounced than that in **2**, see also Scheme 1 that also shows a nice correlation between δ's (^{77}Se) and δ's (^{11}B-antipodal) for SeB_5H_5, 1-SeB_9H_9, and $SeB_{11}H_{11}$. In contrast, there is no such a correlation between δ's (^{77}Se) and δ's (^{11}B-antipodal) for 4-Cl-SeB_5H_4, 10-Cl-SeB_9H_8, and 12-Cl-$SeB_{11}H_{10}$ (r^2 = 0.43).

The coupling constants $^1J(^{77}Se^{11}B)$ are computed to be zero for each of the Se–B and Se···B pairs for all the compounds under scrutiny, obviously due to a very large amount of Se isotopes. Therefore, the coupling constants K are computed instead, *i.e.* exclusively those between the ^{77}Se and ^{11}B nuclei. Since spins of these nuclei differ, *viz* 3/2 for ^{11}B and 1/2 for ^{77}Se, the former exhibits four spin functions with eigenvalues of −3/2, −1/2, 1/2, and 3/2 in contrast to just two such functions for ^{77}Se (−1/2, 1/2). For the algebraic derivation of such function for ^{11}B, see ref. 26. On this basis the coupling constants K (^{77}Se ^{11}B) are relatively small. However, computations of the coupling constants of the J-type between the B atoms were performed (the ^{10}B isotope is also included in the computations) and the values obtained are obviously larger than the K ones.

Interactions in the crystal structure of **1b** were examined using a cluster model around molecule 2 (according to X-ray labeling). Two-body and many-body interaction energy (ΔE^2 and ΔE^{MB}) values were computed between the selected central molecule 2 and two layers of the surrounding molecules (see Fig. 6; individual molecules are labeled as A, B, and C). The surroundings molecules within 5 Å of the central molecule 2 formed the first layer; the second layer was formed by mole-

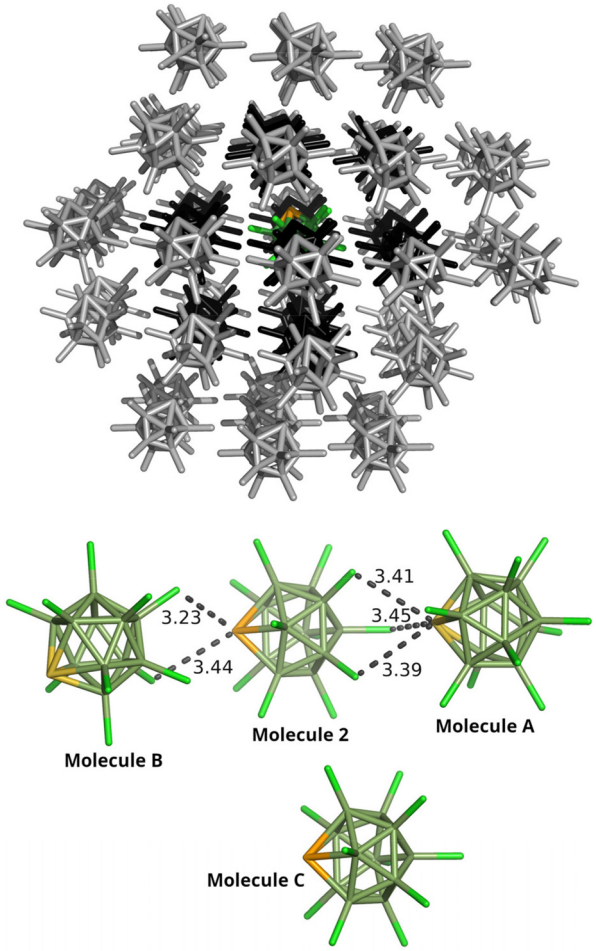

Fig. 6 The cluster model of the reported crystals of *closo*-$SeB_{11}Cl_{11}$ (up). The central molecule is colored by the element: the 1st layer in black and the 2nd layer in gray. The most stable interaction motifs from the crystals (down). Close contacts below the sum of van der Waals radii are in Å. The atom color coding is as follows: orange – selenium, green – chlorine, and forest green – boron.

Table 4 Two-body and many-body interaction energies (ΔE^2 and ΔE^{MB}) computed at the DFT-D3/TPSS/TZVPP level in kcal mol^{-1}

Compound	$\sum\Delta E^2$ (1st layer)	$\sum\Delta E^{MB}$ (1st layer)	$\sum\Delta E^2$ (2nd layer)	Total
$SeB_{11}Cl_{11}$ (**1b**)	−46.87	5.46	−4.09	−45.50

cules within 5 Å of the first layer. The obtained overall binding of molecule 2 is summarized in Table 4. Molecule 1 is expected to exhibit very similar energetic balances. Concerning the energy criteria in the crystals of **1b**, the ΔE^2 values of the most favorable interaction motifs in the reported X-ray crystal structure of **1b** are summarized in Table 5. The chalcogen-bonding motifs (*i.e.* the motifs 2:A and 2:B) had ΔE^2 values of −7.93 and −7.20 kcal mol^{-1} at the DFT-D3 level, thus accounting for about 33% of the total computed binding of **1b**. The SAPT0 decomposition showed that the chalcogen-bonding motifs were stabilized mainly by dispersion, which formed approximately 57% of the attractive terms. The second most important term was electrostatic, forming about 31% of the attractive terms. The remaining motifs had considerably less negative ΔE^2 values with a very large contribution of the dispersion energy (about 84%).

Conclusions

The successful chemistry of chlorinated telluraboranes and pnictogenaboranes initiated the repetition of the vacuum co-pyrolysis of B_2Cl_4 with Se_2Cl_2 at various molar ratios and temperatures in search of the generation of other polyhedral *closo*-selenaboranes than SeB_5Cl_5 (**1a**) and $SeB_{11}Cl_{11}$ (**1b**). Indeed, bicapped square-antiprismatic *closo*-1-SeB_9Cl_9 (**2**) was detected this time by 1- and 2-D ^{11}B NMR spectroscopy and exact mass spectrometry. In addition, vacuum sublimation provided suitable crystals of **1b**, which were successfully diffracted by means of the single-crystal X-ray technique, and the first solid-state structure in the family of chlorinated selenaboranes was determined; in it, the structure of **1b** slightly departs from the symmetry of C_{5v}, apparently due to the corresponding crystal packing. Interestingly, the computations at the DFT-D3 level have revealed that 33% of the total computed binding motifs in the **1b** crystal are caused by very strong chalcogen bonding. The subsequent SAPT decomposition illustrates that the bonding motifs in the crystals are mainly attributable to the dispersion and electrostatic terms. The more refined techniques of ^{11}B NMR and ^{77}Se NMR spectroscopy have resolved the coupling constants and ^{77}Se chemical shifts of **1a** and **1b**, which are in good agreement with their computed values. The extraordinary downfield ^{11}B NMR chemical shift of B(10) in **2** has been ascribed to the intensive paramagnetic contribution to the shielding tensor in this bicapped square-antiprismatic

Table 5 Interaction energies (ΔE^2) computed at the DFT-D3/TPSS/TZVPP and SAPT0/jun-cc-pVDZ levels. ΔE^2 have been decomposed into electrostatic (E_{elec}), exchange (E_{exch}), induction (E_{ind}) and dispersion (E_{disp}) contributions using the SAPT methodology. All energies are in kcal mol^{-1}. The relative values in parentheses show the contribution to the sum of all the attractive terms

	DFT-D3	SAPT0				
		Total	E_{elec}	E_{exch}	E_{ind}	E_{disp}
2:A	−7.93	−9.34	−8.06 (31.7%)	16.06	−2.95 (11.6%)	−14.39 (56.6%)
2:B	−7.20	−8.12	−6.61 (30.6%)	13.46	−2.51 (11.6%)	−12.47 (57.8%)
2:C	−3.98	−3.32	−0.85 (11.6%)	4.00	−0.31 (4.2%)	−6.16 (84.2%)

motif. Attempts at obtaining other perhalogenated heteroboranes and the subsequent structural studies are in progress in our laboratories, in particular, in relation to 2D-aromatic heterocycles.

Conflicts of interest

There are no conflicts to declare.

Acknowledgements

This work was supported by the Czech Science Foundation (project no. 23-05083S). The authors also acknowledge the support by the state of Baden–Württemberg through bwHPC and the German Research Foundation (DFG) through no. INST40/467-1FUGG (Justus cluster).

References

1 R. N. Grimes, *Carboranes*, Academic Press, 3rd edn, 2016.
2 (*a*) R. E. Williams, *Inorg. Chem.*, 1971, **10**, 210; (*b*) K. Wade, *Adv. Inorg. Chem. Radiochem.*, 1976, **18**, 1; (*c*) R. E. Williams, *Adv. Inorg. Chem. Radiochem.*, 1976, **18**, 67; (*d*) R. W. Rudolph, *Acc. Chem. Res.*, 1976, **9**, 446; (*e*) R. E. Williams, in *Electron Deficient Boron and Carbon Clusters*, ed. G. A. Olah, K. Wade and R. E. Williams, Wiley and Sons, New York, 1991, vol. 11; (*f*) R. E. Williams, *Chem. Rev.*, 1992, **92**, 177.
3 D. Hnyk and D. A. Wann, Boron: the Fifth Element, in *Challenges and Advances in Computational Chemistry and Physics*, ed. D. Hnyk and M. L. McKee, 2016, vol. 20, ch. 2.
4 B. J. Eckstein, L. C. Bron, B. C. Noll, M. P. Moghadasnia, G. J. Balaich and C. M. McGuirk, *J. Am. Chem. Soc.*, 2021, **143**, 20207.
5 D. B. Werz, R. Gleiter and F. Rominger, *J. Org. Chem.*, 2004, **69**, 2945.
6 L. Vogel, P. Wonner and S. M. Huber, *Angew. Chem., Int. Ed.*, 2019, **58**, 1880.
7 (*a*) $SeB_{10}H_{12}$ and $Se_2B_9H_9$: J. L. Little, G. D. Friesen and L. J. Todd, *Inorg. Chem.*, 1977, **16**, 869; (*b*) $Se_2B_6H_9^-$, $Se_2B_7H_9$, $SeB_{18}H_{21}^-$, $SeB_{18}H_{19}^-$, $Se_2B_{17}H_{18}^-$, and $Se_2B_{18}H_{19}^-$: J. Bould, M. G. S. Londesborough, M. Litecká, R. Macías, S. L. Shea, T. D. McGrath, W. Clegg and J. D. Kennedy, *Inorg. Chem.*, 2022, **61**, 1899; (*c*) $SeB_{16}H_{18}$: J. Bould, O. Tok, M. Litecká, M. G. S. Londesborough and M. Ehn, *Inorganica Chim. Acta*, 2022, **542**, 121148; (*d*) $Se_2B_9H_{10}^-$: J. Bould, O. Tok, W. Clegg, M. G. S. Londesborough, M. Litecká and M. Ehn, *Inorganica Chim. Acta*, 2023, **547**, 121341; (*e*) $SeB_{11}H_{11}$: D. Hnyk, D. A. Wann, J. Holub, M. Bühl, H. E. Robertson and D. W. H. Rankin, *Dalton Trans.*, 2008, **1**, 96; (*f*) $SeB_9H_{12}^-$ and SeB_9H_9: G. D. Friesen, R. L. Kump and L. J. Todd, *Inorg. Chem.*, 1980, **19**, 1485.
8 W. Keller and M. Hofmann, *Z. Anorg. Allg. Chem.*, 2017, **643**, 729.
9 For a selected review on the boron subhalides B_nX_n, see: J. A. Morrison, in *Advances in Boron and the Boranes*, ed. J. F. Liebman, A. Greenberg and R. E. Williams, VCH Publishers, New York, 1988, 151.
10 (*a*) W. Haubold, W. Keller and G. Sawitzki, *Angew. Chem., Int. Ed. Engl.*, 1988, **27**, 925; (*b*) W. Keller, L. G. Sneddon, W. Einholz and A. Gemmler, *Chem. Ber.*, 1992, **125**, 2343; (*c*) W. Keller, W. Einholz, D. Rudolph and Th. Schleid, *Z. Anorg. Allg. Chem.*, 2017, **643**, 664; (*d*) W. Keller, G. Sawitzki and W. Haubold, *Inorg. Chem.*, 2000, **39**, 1282; (*e*) W. Keller, *Z. Anorg. Allg. Chem.*, 2017, **643**, 517.
11 W. Keller, J. Conrad and M. Hofmann, *ChemistrySelect*, 2023, **8**, e202301653.
12 W. Keller, J. Ballmann, M. B. Sárosi, J. Fanfrlík and D. Hnyk, *Angew. Chem., Int. Ed.*, 2023, **62**, e202219018.
13 M. Lamoureux and J. Milne, *Can. J. Chem.*, 1989, **67**, 1936.
14 R. Weinmann, PhD Thesis, Universität Stuttgart, 1985.
15 J. Holub, J. Vrána, A. Růžička, Z. Růžičková, J. Fanfrlík and D. Hnyk, *ChemPlusChem*, 2019, **84**, 822.
16 P. v. R. Schleyer and K. Najafian, *Inorg. Chem.*, 1998, **37**, 3454.
17 D. Hnyk, D. A. Wann, J. Holub, S. Samdal and D. W. H. Rankin, *Dalton Trans.*, 2011, **40**, 5734.
18 (*a*) D. Hnyk, E. Vajda, M. Bühl and P. v. R. Schleyer, *Inorg. Chem.*, 1992, **31**, 2464; (*b*) H. Møllendal, S. Samdal, J. Holub and D. Hnyk, *Inorg. Chem.*, 2003, **42**, 3043.
19 P. Melichar, D. Hnyk and J. Fanfrlík, *Phys. Chem. Chem. Phys.*, 2018, **20**, 4666.
20 W. Keller, M. Hofmann, M. B. Sárosi, J. Fanfrlík and D. Hnyk, *Inorg. Chem.*, 2022, **61**, 16565.
21 T. Clark, M. Hennemann, J. S. Murray and P. Politzer, *J. Mol. Model.*, 2007, **13**, 29.
22 A. Pecina, M. Lepšík, D. Hnyk, P. Hobza and J. Fanfrlík, *J. Phys. Chem. A*, 2015, **119**, 1388.
23 J. Holub, P. Melichar, Z. Růžičková, J. Vrána, D. A. Wann, J. Fanfrlík, D. Hnyk and A. Růžička, *Dalton Trans.*, 2017, **46**, 13714.
24 Such a value of $V_{s,max}$ is responsible for the S···Ph contact (chalcogen bonding) in the crystal, see: J. Fanfrlík, A. Přáda, Z. Padělková, A. Pecina, J. Macháček, M. Lepšík, J. Holub, A. Růžička, D. Hnyk and P. Hobza, *Angew. Chem.*, 2014, **126**, 10303.
25 See, *e.g.*M. Bühl, W. Thiel, U. Fleischer and W. Kutzelnigg, *J. Phys. Chem.*, 1995, **99**, 4000.
26 J. Macháček, M. Bühl, J. Fanfrlík and D. Hnyk, *J. Phys. Chem. A*, 2017, **121**, 9631.